BASIC RESEARCH

WILEY

Wet surface wall model for latent heat exchange during evaporation

Kiao Inthavong[1] ⓘ　|　David F. Fletcher[2] ⓘ　|　Mehrdad Khamooshi[1] ⓘ　|
Sara Vahaji[1] ⓘ　|　Hana Salati[1] ⓘ

[1]Mechanical and Automotive Engineering, School of Engineering, RMIT University, Bundoora, Victoria, Australia

[2]School of Chemical and Biomolecular Engineering, The University of Sydney, Sydney, New South Wales, Australia

Correspondence
Kiao Inthavong, Mechanical and Automotive Engineering, School of Engineering, RMIT University, Bundoora, VIC 3083, Australia.
Email: kiao.inthavong@rmit.edu.au

Abstract

Air conditioning is a dual heat and mass transfer process, and the human nasal cavity achieves this through the mucosal wall surface, which is supplied with an energy source through the sub-epithelial network of capillaries. Computational studies of air conditioning in the nasal cavity have included temperature and humidity, but most studies solved these flow parameters separately, and in some cases, a constant mucosal surface temperature was used. Recent developments demonstrated that both heat and mass transfer need to be modeled. This work expands on existing modeling efforts in accounting for the nasal cavity's dual heat and mass transfer process by introducing a new subwall model, given in the Supplementary Materials. The model was applied to a pipe geometry, and a human nasal cavity was recreated from CT-scans, and six inhalation conditions were studied. The results showed that when the energy transfer from the latent heat of evaporation is included, there is a cooling effect on the mucosal surface temperature.

KEYWORDS
CFD, drug delivery, nasal cavity, nebulizer, transient

1 | INTRODUCTION

Among the physiological capabilities of the nose, one crucial function is the ability of the nasal cavity to sufficiently condition the inhaled air to near alveolar conditions, that is, body core temperature and saturated air. In most cases, the air is heated with humidification, but the air may need to be cooled and humidified under hot environmental conditions. The dual heat and mass transfer processes are achieved by the mucosal wall surface supplied with an energy source through the sub-epithelial network of capillaries.

In vivo air temperature measurements within the nasal cavity are challenging due to the invasive nature of thermo-couples placed inside the complex anatomy that exhibit very narrow nasal passageways. This limits the ability to measure spatial temperature distribution and time resolution accurately. Nevertheless, studies have reported temperature, and relative humidity measurements in different regions of the nasal cavity at the end of inspiration,[1–3] and at the end of expiration.[4,5] These measurements provide baseline temperature and humidity values for generalizing the changes in respired air.

In nasal cavity geometries subjected to surgery, the confined airway space is altered and ultimately influences the heat and mass transfer process. Tsakiropoulou et al.[6] found a 13% reduction in the heating capacity of the air at the inferior turbinate and 19% reduction at the middle turbinate. No humidity difference was observed. Lindemann et al.[7] found statistically significant lower humidity and temperatures in the nasopharynx region in patients that underwent unilateral radical sinus surgery. However, in patients that underwent septoplasty with turbinoplasty,[8] and closure of nasal septal perforations,[9] heating and humidification were improved. While in patients with chronic rhinosinusitis that underwent sinus surgery, no changes in temperature or humidity were observed.[10]

Computational studies have been performed extensively to evaluate the air conditioning capability[11–19] where the results demonstrated the heat transfer effects producing logarithmic temperature profiles associated with heat transfer in an internal pipe flow with a constant surface temperature boundary condition. Some studies included the effects of surgery.[20,21] Dayal et al.[22] reported that nasal heating and humidification efficiencies decreased significantly after virtual resection of the middle turbinate. Garcia et al.[23] demonstrated that an atrophic nose did not condition inspired air as effectively as the healthy geometries. In these studies, temperature and humidity were solved separately, and at the wall, a constant surface temperature and water vapor concentration defined by a species mass fraction of H_2O were used as the boundary conditions.

The water vapor concentration at the mucus-air interface as a function of an energy balance was first modeled in Kumahata et al.,[24] where the temperature and humidity of the inhaled air were adjusted by heat and mass (e.g., water) exchange between the epithelium side of the mucosal wall containing capillaries and the air side of the nasal cavity via a mucous membrane thickness covering the nasal cavity wall. A similar approach was adopted by Kim et al.[25] and Chung and Na[26] where a sub-wall model was used.

However, in the computational studies cited, the effect of latent heat was excluded. Hanida et al.[27] extended the work of Kumahata et al.[24] and included both sensible and latent heat, which influences temperature and relative humidity of the air inside the nasal cavity. Their approach produced two separate but coupled sub-wall models for the heat and water vapor (humidity) exchange. Inspired by the Hanida et al.[27] model, this study improves their approach by creating a single sub-wall model that couples the heat and mass transfer at the mucus-air interface instead of using two sub-wall models while better representing the submucosal anatomy. The new model, implemented in Ansys Fluent 2021R1, updates the past capability to current contemporary computational modeling techniques.

2 | METHOD

2.1 | Geometries

A straight pipe section was created for demonstrating the sub-wall model. The pipe diameter was 0.012 m split into two zones - the main fluid zone and a thin solid zone. The solid zone thickness can be arbitrary if an effective thermal resistance is applied to obtain the heat flux through the solid. Furthermore, since it is a solid zone with a heat diffusion process, only two prism layers are needed to establish the energy flux across the solid–fluid interface. Figure 2A demonstrates the pipe geometry which contains a polyhedral mesh in the core fluid region, six prism layers in the near wall region, and two prism layers in the solid zone. The pipe diameter was 11.8 mm, while the outer annular solid zone was 0.1 mm thick.

A human nasal cavity model was reconstructed from CT scans of a healthy 25-year-old, Asian female (161 cm height, 53 kg mass, without nasal septum deviation, turbinate hypertrophy and sinusitis. This model has been used in previous studies in Shrestha et al.,[28] Zhang et al.[29]) at rest condition. The CT data were obtained from a Siemens Dual Source CT Machine, where the scan parameters were 0.39×0.39 mm^2 at 512×512 pixel resolution, with 0.5 mm slice thickness. The surface geometry, anatomy, and coronal cross-section slices are shown in Figure 2A,B depicting a polyhedral surface mesh. The cells adjacent to the surface comprised two prism layers representing the solid zone and five prism layers inside the fluid zone. A solid–fluid wall interface separated the two zones. Polyhedral cells were used to connect the hexahedral cells to the prism layers in the fluid zone, thus forming the poly-hexcore meshing.

2.2 | Sub-wall model

The two zonal sub-wall model developed by Kumahata et al.[24] employed a two-film theory to evaluate the mass from species transport to overcome Ansys-Fluent's inability to specify a Neumann boundary condition for the mass transfer,

depicted in Figure 1. Their proposed model involved mass transfer across a surface area, where the mass was produced from an organ/anatomy surface, and diffusing through a membrane given as:

$$w_{\mathrm{memb}} = D_{\mathrm{memb}} \frac{(Y_0 - Y_s)}{\delta_{\mathrm{memb}}} \rho \tag{1}$$

where w is the mass flux; $D_{\mathrm{memb}} = 2.6 \times 10^{-5}$ m^2/s is the mass diffusivity; $Y_0 = 0.034$ was a constant mass fraction representing a fully saturated state at 34°C; Y_s is the boundary mass fraction; and δ_{memb} is the membrane thickness which was evaluated from a list of values from 1.0 to 5.0 mm. For dimensional equality, we added the density term ρ to the right hand side of the equation that is not given in Kumahata et al..[24] The computational fluid dynamics (CFD) modeled region takes the mass transfer through a boundary layer defined as:

$$w_{\mathrm{bl}} = D_{\mathrm{bl}} \frac{(Y_s - Y)}{\delta_{\mathrm{bl}}} \rho \tag{2}$$

where $D_{\mathrm{bl}} = 3.0 \times 10^{-5}$ m^2/s, under the assumption that the water vapor diffusion is stronger in the boundary layer than in the membrane. A similar approach was proposed in earlier work by Kim et al.,[25] Chung and Na,[26] Na et al..[30] The fluxes are continuous, so that $w_{\mathrm{memb}} = w_{\mathrm{bl}}$, and therefore the flux at the solid-air interface, F_s can be determined. The latent heat transport was added by Hanida et al.[27] by taking the product of the mass flux F_s with the heat of vaporization term.

We propose an updated model that calculates the mass flux at the air-mucus interface, where the mucosal surface is assumed wet and therefore the water vapor state is fully saturated (Figure 1C,D). This differs from the original model by Kumahata et al.[24] which assumed a fully saturated state at an organ surface, where mass transfer takes place in the membrane and boundary layer regions, and therefore the water-vapor at the boundary layer-air interface is not fully saturated. The water vapor fraction is a function of temperature (plotted in Figure 1B), given as:

(A) Kumahata etl a. (2010)'s water exchange model using a two-film theory

(B) Water vapour fraction equation defining $w(t)$ in eqn.3

(C) Schematic of the nasal sub-mucosal anatomy

(D) CFD representation of a two-zonal air-submucus model
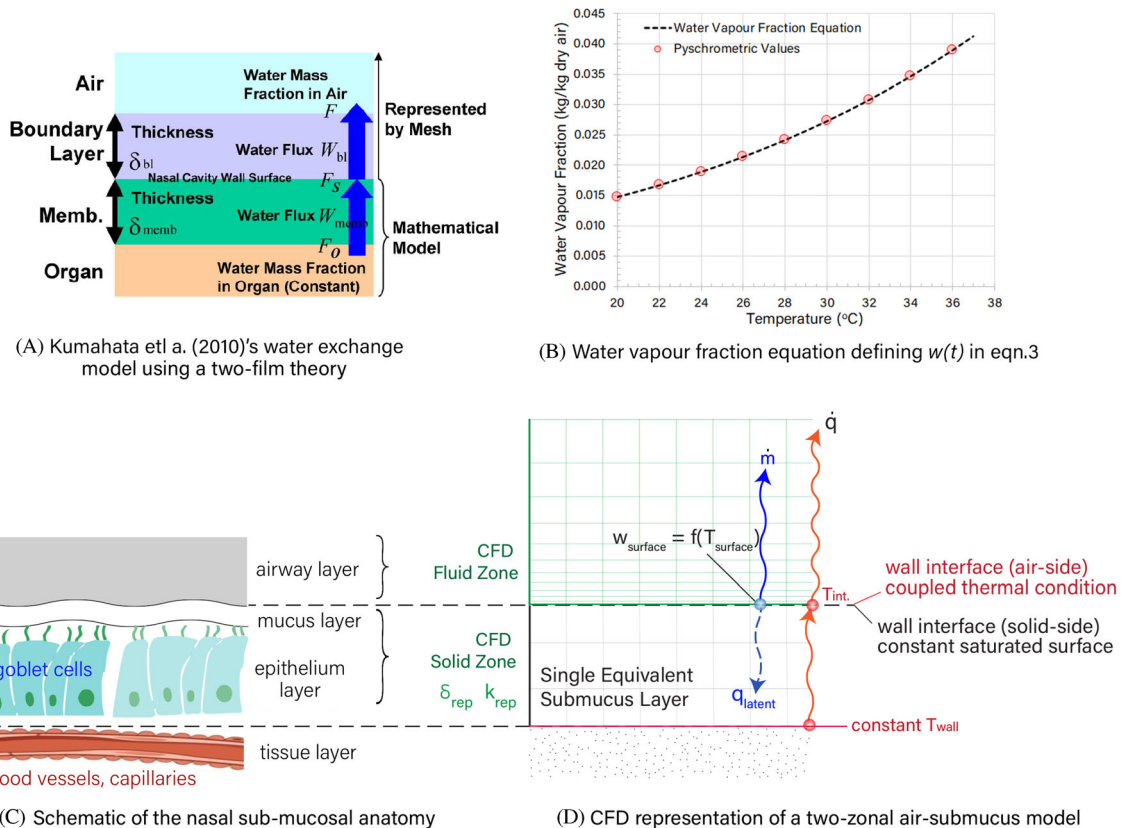
FIGURE 1 Development of the subwall model accounting for latent heat effects

$$w_{\text{surf}}(T) = \frac{1}{1000}\left(0.0006312 * T^3 - 0.010972 * T^2 + 0.6036 * T + 2.027\right) \tag{3}$$

where T is temperature in Celsius and w_{surf} is the water vapor fraction per kg of dry air.

Figure 1D shows a fluid zone representing the air region of the nasal cavity and a solid zone that represents the submucosal wall region. At the base of the solid zone is a constant wall temperature of $T_{\text{wall}} = 37°C$ based on the underlying blood vessels that provide body core temperatures which is widely accepted to be between 36.5 and 37.4°C in the normal range. This temperature was applied along the region in the main nasal passages from plane y1 posteriorly to the nasopharynx outlet, while $T_{\text{wall}} = 34°C$ in the vestibule region (see Figure 2B for the locations). This setting is not equal to the body-core temperature and susceptible to external environmental condition in reality, as demonstrated in recent work that have applied this value.[2,4,11,13,19] The submucus-epithelial zone has a representative thickness δ_{rep} and is based on the solid zone geometry (see Figure 1). The conduction heat transfer is governed by:

$$\dot{q} = k\frac{\Delta T}{\delta} = \frac{\Delta T}{\Delta R_{\text{eff}}} \tag{4}$$

where,

$$R_{\text{eff}} = \frac{\delta_{\text{rep}}}{k_{\text{rep}}} \tag{5}$$

(A) Pipe Geometry
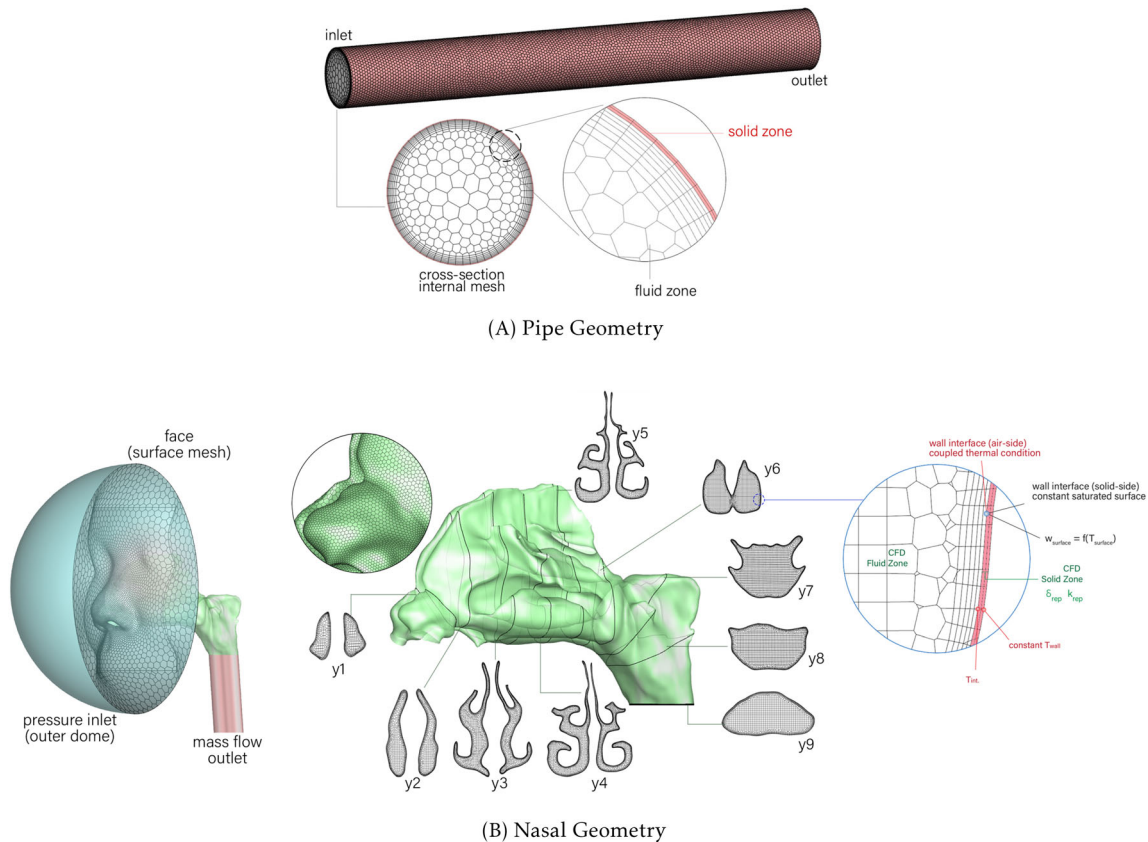
(B) Nasal Geometry

FIGURE 2 Computational geometry and mesh of (A) pipe geometry; (B) nasal geometry showing the surface and internal mesh where a zoomed region of the near wall mesh of plane y6 shows the internal solid and fluid zones, and is labeled with parameters related to the subwall model. The constant wall temperature was $T_{\text{wall}} = 37°C$ for the main nasal passages from plane y1 posteriorly to the nasopharynx outlet, while $T_{\text{wall}} = 34°C$ in the vestibule region

where R_{eff} is the effective thermal resistance. During preliminary testing a $R_{eff} = 0.006$ K/W m² was the most suitable value, based on conductivity and thickness parameters suggested in Na et al.[30] who reviewed anatomic information on the respiratory mucosa from Beule,[31] and later in Senanayake et al..[32] The k_{rep} is a representative conductivity for the solid region defined such that the desired effective thermal resistance, R_{eff}, per unit area (K/W m²) was achieved. For example, in the pipe geometry, we set $k_{rep} = 0.1667$ W/mK for a $\delta_{rep} = 0.001$ m, giving $R_{eff} = 0.006$ K/W m².

The mass flux across the mucus-air interface is determined from the species transport equation, and is used to determine the latent heat of evaporation given by,

$$\dot{Q} = w h_{fg}$$

where the h_{fg} is the latent heat of vaporization in kJ/kg defined as:

$$h_{fg} = 2500.8 - 6.1434 \times 10^{-6} T^3 + 1.5893 \times 10^{-3} T^2 - 2.3641 T$$

and T is temperature in °C. The mass transfer from the mucus into the air leads to an energy loss, absorbed at the liquid interface, and subsequently a change in the temperature is observed. A User Defined Function was used to implement the model (details and instructions for its use are given in the Supplementary Material S1).

2.3 | Fluid and species transport modeling

The flow equations describing the conservation for mass, momentum, energy, and water vapor species are expressed as:

$$\frac{\partial}{\partial x_i}(\rho u_i) = 0 \tag{6}$$

$$\frac{\partial}{\partial x_j}(\rho u_i u_j) = -\frac{\partial p}{\partial x_i} + \frac{\partial \sigma_{ij}}{\partial x_j} \tag{7}$$

$$\frac{\partial}{\partial x_i}(u_i \rho C_p T) = \frac{\partial}{\partial x_i}\left(k\frac{\partial T}{\partial x_i}\right) + \frac{\partial}{\partial x_i}\left(\sum_{i=1}^{n}(h_i j_i)\right) \tag{8}$$

$$\frac{\partial u_i C}{\partial x_i} = \frac{\partial}{\partial x_i}\left(D\frac{\partial C}{\partial x_i}\right) \tag{9}$$

where u_i is the flow velocity vector, p is the pressure, σ_{ij} is the stress tensor due to molecular viscosity, T is temperature, k is thermal conductivity, C_p is the specific heat capacity, h_i is the species enthalpy, j_i is species diffusion flux and D is the mass diffusivity.

2.4 | Numerical solution settings

The spatial discretization applied was second-order for all equations while the least-squares cell-based method was used for the gradient discretization, which evaluated gradients within each cell. The Warped-Face Gradient Correction option was used, which adjusts the gradient discretization method to improve the gradient accuracy for cells that may be deformed, have high aspect ratios, or non-flat faces.

The "coupled" scheme was used for the pressure–velocity coupling, as when the SIMPLE algorithm was used simulations had a tendency to diverge. In the coupled approach, the mass and momentum equations are solved simultaneously and convergence is achieved using a pseudo transient approach that leads to better stability. The pseudo-transient time scales for the fluid and solid zones were set to 0.001 s, where larger values led to divergence. The

evaporation flux across the solid-air interface from the subwall model was calculated every third iteration (using an "execute-on-demand" function), which was a compromise between speed and stability of the iterative solution. In addition to the residuals, the mass-weighted average of the temperature and water fraction was evaluated at the outlets to monitor the solution convergence.

2.5 | Heat and mass transfer cases

For the pipe flow, the inlet and surface temperature were set to 50°C, while the inlet humidity was set as a dry condition with $w = 0$. This condition mimics an adiabatic saturation process (i.e., evaporative cooling process), where the evaporation from the wet solid surface to the air occurs. The evaporation increases the moisture content of the air, and the air temperature decreases since part of the latent heat of vaporization of the water that evaporates comes from the air. Heat transfer does not occur because the air and surface temperatures are equal, and therefore a temperature drop in the fluid must come from the latent heat transfer.

For the nasal cavity model, the steady state flow simulations were setup as closely to the experimental measurements of.[3] The three conditions were $T = 19.5°C$ at 5 L/min; $T = 10.5°C$ at 10 L/min; and $T = 0.8°C$ at 20 L/min. Three additional cases were investigated: "cold dry air" (CDA) $T = 12°C$ and 13%RH (relative humidity); "normal air" (NORM) $T = 25°C$ and 35%RH and; "hot humid air" (HHA) $T = 35°C$ and 80%RH, at a flowrate of 15 L/min.

3 | RESULTS

3.1 | Evaporative cooling effect inside a wet internal pipe

Heat and mass transfer along the pipe is shown in Figure 3 through contours taken at the mid-cross-section plane of the pipe, where the air temperature contours in the mid-plane and y-planes (axial planes) decreased as a result of the latent heat. When the latent heat is excluded, there is no change in the sensible heat transfer the air temperature. The moisture transfer occurs between the solid–fluid interface, and diffusion into the flow field is evident by the relative humidity gradient occurring in the near-wall region. The effect of latent heat energy transfer on moisture diffusion is visually imperceptible through the contours but is elucidated by the line plots that demonstrate a greater relative humidity when latent heat transfer is neglected.

The temperature and humidity profiles were taken along vertical lines at cross-sections at $y = 25$, 50, and 75 mm. The inclusion of latent heat showed a gradual temperature change from the uniform inlet temperature profile of 50°C. There is only a slight difference between the humidity profiles when latent heat effects are included.

Figure 4 shows the temperature contour at the solid-air interface, demonstrating the cooling effect from evaporation. The temperature at the start of the interface is cooled to 27°C and increases due to the solid wall and flow temperature of 50°C. The solid-air interface is representative of any wet surface with an underlying sub-surface region that is infinitely wet. For example, the surface of a pool of water or, in the context of this study, the mucosal surface of the human nasal cavity, is treated as a fully saturated surface that is replenished by the submucosal epithelial cells. There is no sensible heat transfer in the absence of latent heat energy transfer since the initial temperatures are all identical.

3.2 | Heat and mass transfer in the human nasal cavity model

Rouadi et al.[3] applied a constant flow of air through the nasal cavity with a temperature probe located at the nasopharynx. These values were compared with simulations on the nasal cavity model with and without latent heat. The temperature along the base of the nasal cavity wall boundary is set to $T = 37°C$, representing core-body temperatures, and that of the nasal vestibule was set to $T = 34°C$, slightly lower based on its external location to the internal nasal cavity. The lower vestibule temperature was based on its surface being susceptible to external environmental conditions.

The mucus surface temperature contour is shown in Figure 5, which shows a variation in mucosal temperature of up to 20°C (for $T_{inlet} = 0.8°C$). The large temperature variation suggests a constant temperature boundary condition setting for the nasal cavity walls is unsuitable. The effects of latent heat is consistent in all cases where there is additional
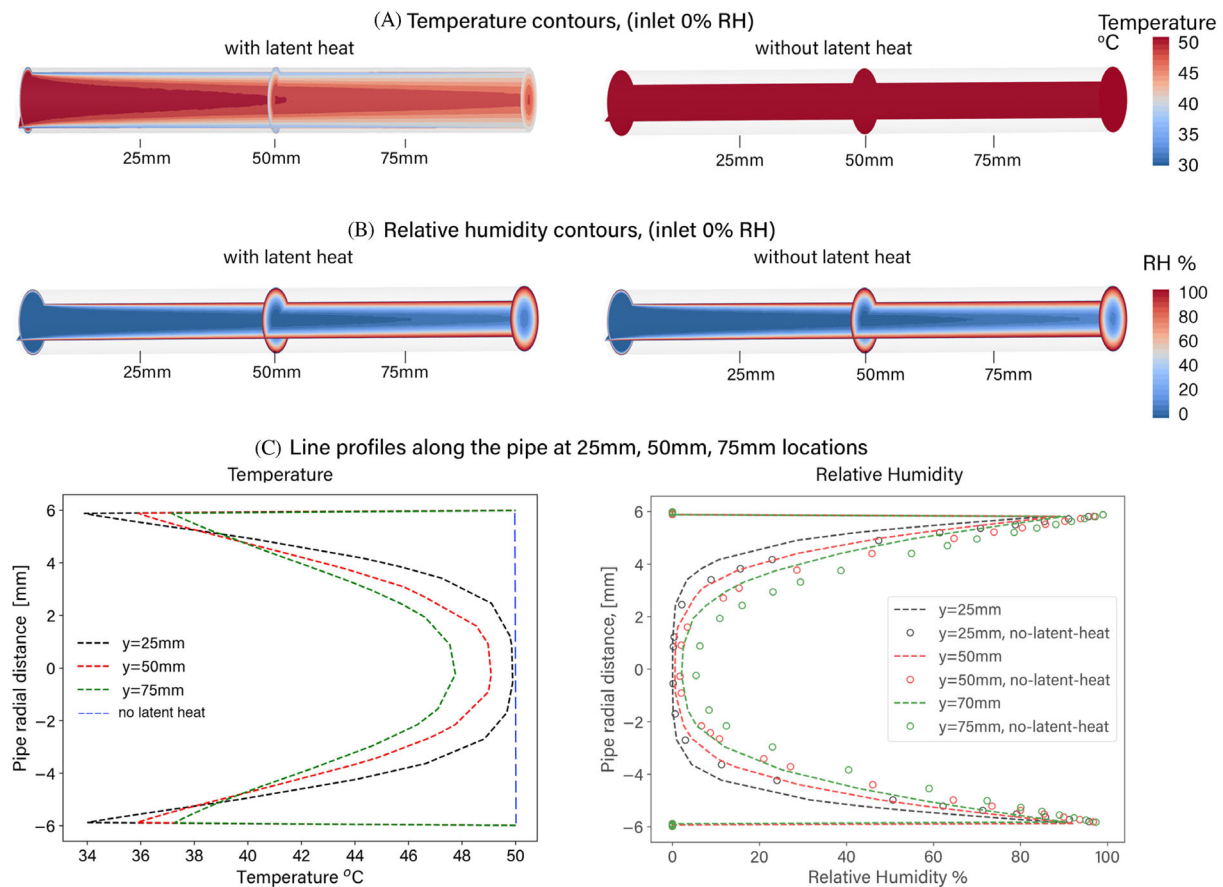
FIGURE 3 Heat and mass transfer through a circular straight pipe. Left-hand-side images represent modeling with latent heat, and right-hand-side images represent modeling without latent heat. (A) Temperature contours with Re = 1000, u_{ave} = 1.2 m/s. (B) Relative humidity contours. (C) Line profiles at taken along the center of each cross-section at y = 25, 50, and 75 mm
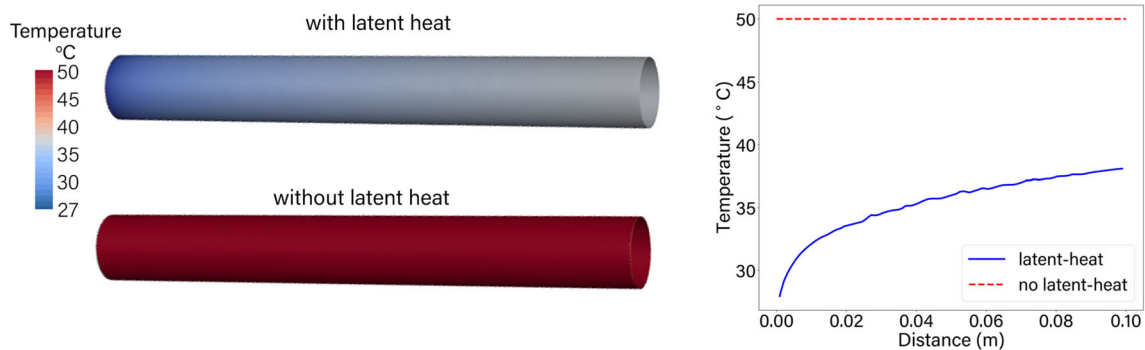
FIGURE 4 Solid-air interface temperature in the pipe demonstrating the evaporative cooling effect from latent heat of vaporization

cooling, along the lateral walls (where the airflow passes over the surfaces), compared with the no latent heat cases. The mucosal surface temperatures are the coolest in the regions where the air flows over the surfaces.

Temperature values (mass-weighted-averaged) at planar slices in the coronal axis were calculated, shown in Figure 6. The two models performed similarly in the anterior half when the inlet temperature was highest. In the posterior region and where the inlet temperature was $T = 0.8°C$ where the inclusion of latent heat provided an evaporative cooling effect at the air-mucus interface.

The nasopharynx temperature was taken at slice $y7$ (location depicted in Figure 2B) and falls within the range of measured data of Rouadi et al..[3] The latent heat model provides a cooling effect at the solid-air interface, leading to cooler temperatures compared with the no latent heat models. The variation in the water vapor fraction (also known as
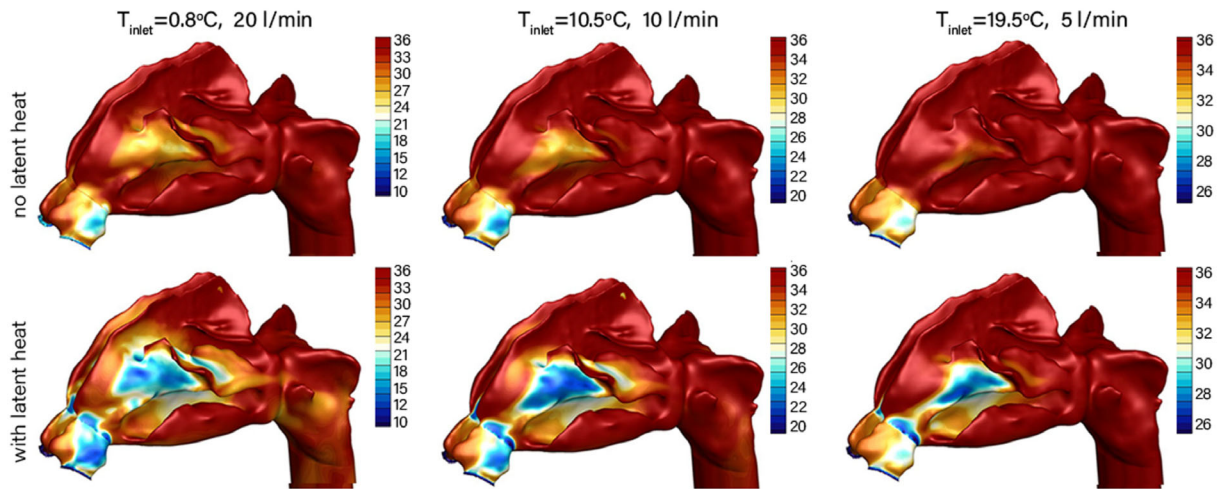
FIGURE 5 Variation in the solid-air interface (mucosal surface) temperature contours for steady state flow cases replicating measurements from Rouadi et al.,[3] where the cases exhibited $T_{in} = 0.8$, 10.5, and 19.5°C

(A) Temperature Profile

(B) Temperature Difference

(C) Water Vapour Fraction

(D) Water Vapour Fraction Difference
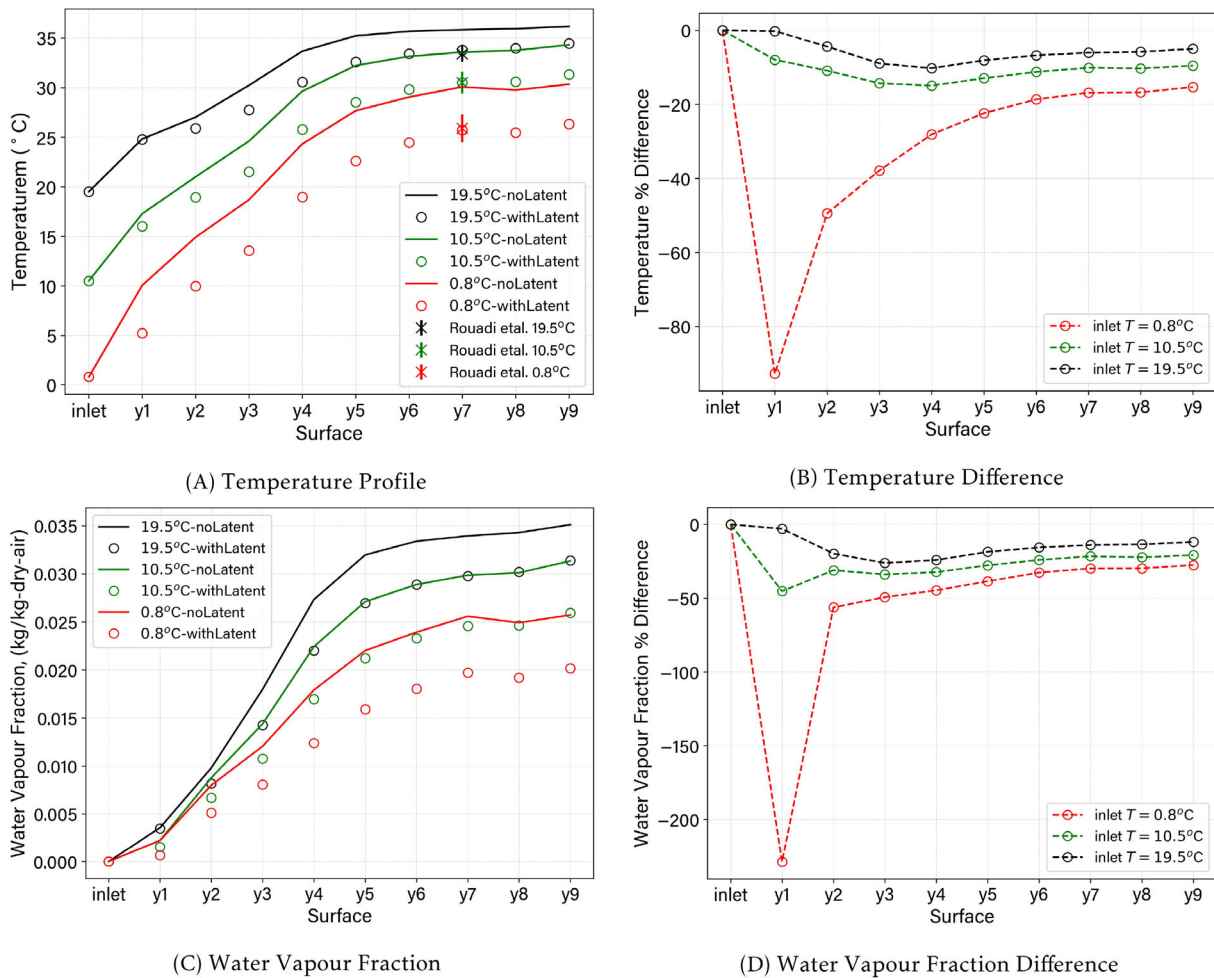
FIGURE 6 (A) Temperature values, mass-weighted over each surface cross-section. (B) Temperature difference between latent heat and no latent heat model. (C) Water vapor mass fraction over each surface cross-section. (D) Difference in water vapor values between latent heat and no latent heat model. The data are obtained for steady state flow cases replicating measurements from Rouadi et al.[3]

specific humidity) is shown in Figure 6C. The difference in the mass transfer is most significant in the posterior region, where there is a difference of 0.002 kg/(kg-dry-air).

The differences in temperature and water vapor between the latent and no-latent models were computed as $(\phi_{latent} - \phi_{noLatent})/\phi_{latent}$ as a percentage. The temperature and water vapor values in the anterior region were low, which causes high percentage changes when the low values are used as a reference. Nevertheless, the average difference in values due to the latent heat model from the middle to posterior region (slice $y3$ to $y9$) was 22% for temperature, and 50% for water vapor.

The mucus surface temperature contour for three inhalation cases: cold dry air (12°C, 13% RH), normal (25°C, 35% RH) and HHA (35°C, 80% RH) at a constant inhalation flow of 15 L/min is shown in Figure 7. While the image demonstrates a subtle difference in the temperature contours posteriorly, there is large discrepancies in the anterior and middle regions, primarily found along the surface region where the inhaled air passes through.

The mean air temperature and water vapor fraction passing through the nasal cavity on the coronal cross-sections are given in Figure 8. The cooling effect for the latent heat model is less significant in the anterior regions and is more significant in the posterior regions. The average difference in values due to the latent heat model from the middle to posterior region (slice $y3$ to $y9$) ranged from 2% to 14% for temperature, and 5%–33% for water vapor.

The plotted data in tabulated form are provided as a single spreadsheet file in the supplementary materials S1.
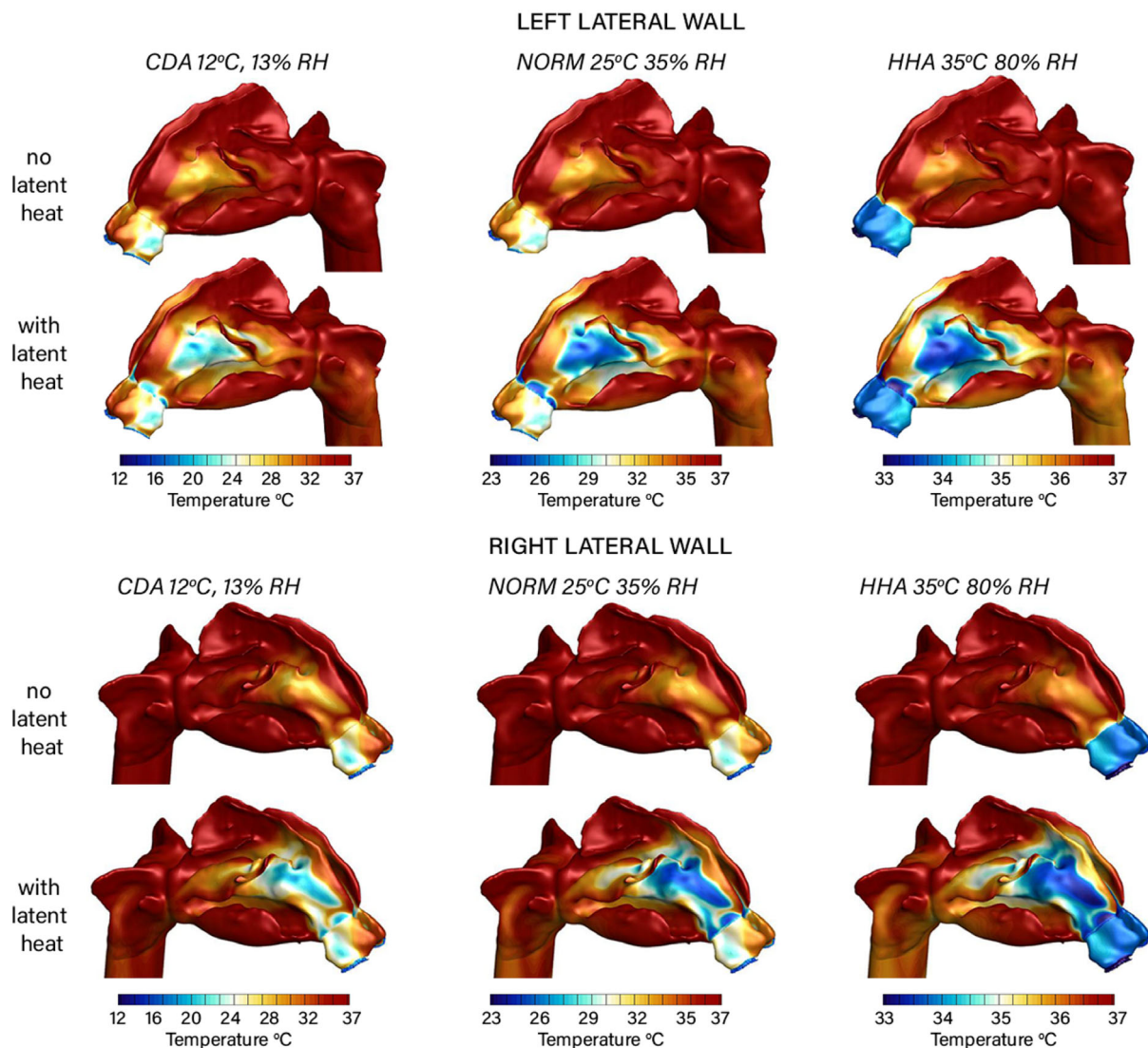
FIGURE 7 Variation in the solid-air interface (mucosal surface) temperature contours for three inhalation conditions: Cold dry air (CDA), $T = 0.8°C$, 13% RH; Normal air (NORM), $T = 25°C$, 35% RH; Hot humid air (HHA), $T = 35°C$, 80% RH

(A) Temperature Profile

(B) Temperature Difference

(C) Water Vapour Fraction

(D) Water Vapour Fraction Difference
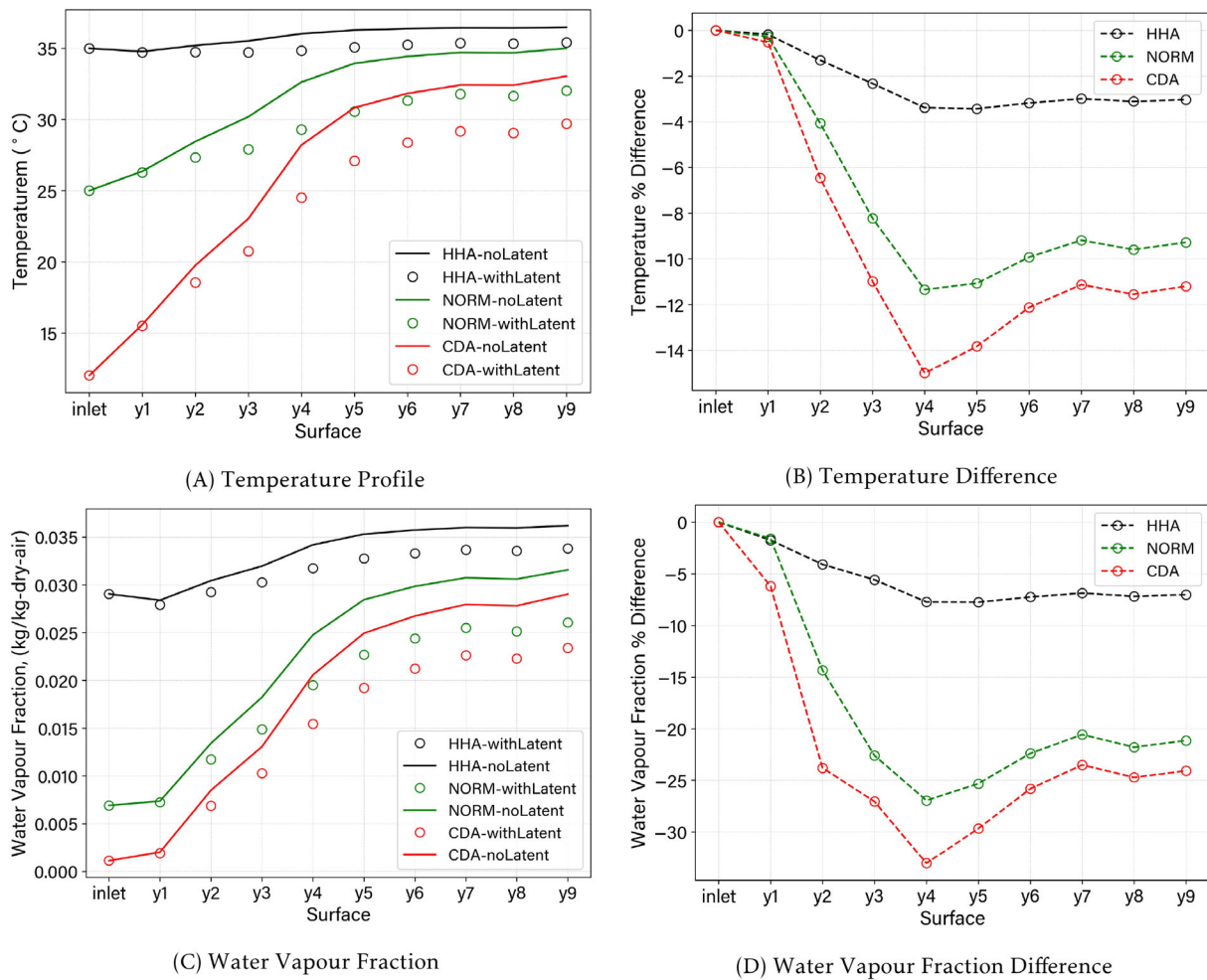
FIGURE 8 (A) Temperature values, mass-weighted over each surface cross-section. (B) Temperature difference between latent heat and no latent heat model. (C) Water vapor mass fraction over each surface cross-section. (D) Difference in water vapor values between latent heat and no latent heat model. The data are obtained for steady state flow cases for three inhaled conditions, cold dry air (CDA), normal air (NORM), and hot humid air (HHA)

4 | DISCUSSION

We propose an updated subwall model that represents a wet surface wall model for latent heat exchange during evaporation. Our model calculates the mass flux at the air-mucus interface, where the mucosal surface is wet and fully saturated, differing from the previous model by Hanida et al.[27] which assumed a fully saturated state along the organs underneath mucus layer thus, the water-vapor at the boundary layer-air interface is not fully saturated.

For evaporation to occur from the mucosal surface, there is a chemical potential differential in the form of concentration gradient of the water vapor, where the water moves from higher potential to lower potential. This can be related to the particle number of the water vapor species of the air, defined by its mass fraction. During inhalation, the chemical potential of water vapor in the inhaled air (unsaturated state at lower temperature) is much less than that on the mucus surface (fully saturated state at higher temperature), leading to a moisture transfer from the surface to the air. The air conditioning capacity of the human nose can be calculated based on the sensible heat energy, air temperature change, and latent heat energy from the water mass transfer from the mucus layer to the inhaled air.

The sensible heat is given by $\dot{Q} = \dot{m}C_p(T_{out} - T_{in})$ where Keck et al.[1] found a temperature difference of $T_{\text{nasopharynx}} - T_{in} = 34-25 = 9°C$. Under the assumption of a tidal volume of 550 ml per inhalation[33] over an inhalation time of 1.65 s, an estimate of the average sensible heat energy transfer rate is:

TABLE 1 Sensible heat energy and latent heat energy during steady inhalation

	Cases from Rouadi et al.[3]			Current CFD results		
	5 L/min $T_{in} = 19.5°C$	10 L/min $T_{in} = 10.5°C$	20 L/min $T_{in} = 0.8°C$	CDA $T_{in} = 12°C$	NORM $T_{in} = 25°C$	HHA $T_{in} = 35°C$
ΔT (°C)	14.95	20.8	25.5	17.7	7.0	0.4
$\dot{Q}_{sensible}$ (W)	1.5	4.3	10.5	5.4	2.1	0.1
	5 L/min $RH_{in} = 0\%$	10 L/min $RH_{in} = 0\%$	20 L/min $RH_{in} = 0\%$	CDA $RH_{in} = 13\%$	NORM $RH_{in} = 35\%$	HHA $RH_{in} = 80\%$
Δw (g/kg)	31	26	20	22	19	5
$\dot{Q}_{latent}$ (W)	7.8	12.9	20.0	16.6	14.2	3.6

$$\dot{Q}_{sensible} = \left(\frac{550 \times 10^{-6} \, [\text{m}^3]}{1.65 \, [\text{s}]} \rho \, [\text{kg/m}^3]\right) 1005 \, [\text{J/kg}°\text{C}] \, (34 - 25) \, [°\text{C}] \tag{10}$$
$$= 3.7 \, [\text{W}]$$

while the humidity changed from an inhaled state of 8.02–32.06 g/m^{3,2,34} giving an approximate latent heat energy transfer rate of,

$$\dot{Q}_{latent} = \left(\frac{550 \times 10^{-6} \, [\text{m}^3]}{1.65 \, [\text{s}]} \times \left(\frac{32.06 - 8.06}{1000}\right) [\text{kg/m}^3]\right) 2431 \, [\text{kJ/kg}] \tag{11}$$
$$= 23.8 \, [\text{W}]$$

In this study, six inhalation conditions were investigated and the temperature change from the inlet to the nasopharynx (airway outlet at location y9) ranged from 14.95 to 25.5°C in the three cases from Rouadi et al.,[3] and 0.4°C for hot humid air to 17.7°C for cold dry air, while the increase in water vapor fraction ranged from 5 to 31 g/kg-dry-air for the six scenarios. Applying Equations (10) and (11) the energy contributions from sensible and latent heat are given in Table 1.

The heat and mass transfer quantities from the six inhalation conditions of this study ($\dot{Q}_{sensible} = 0.1$ to 10.5 W; $\dot{Q}_{latent} = 3.6$ to 20.0 W) agree well with the experimental data of Keck et al.[2] ($\dot{Q}_{sensible} = 3.7$ W; $\dot{Q}_{latent} = 23.8$ W). The results demonstrated the contribution of latent heat energy is 2× (for $T_{in} = 0.8°C$) to 36× (for $T_{in} = 35°C$) greater than sensible heat energy. The energy needed to evaporate the water is taken from the air in the form of sensible heat, leading to an overall cooling effect which was most significant when the inlet humidity was lowest. The evaporative cooling effect is most significant when the temperature difference between the inhaled air and the mucosal surface temperature is low, exemplified by the hot humid air case where $T_{in} = 35°C$. In all the cases, the mucosal surface experienced a cooler temperature when latent heat is included, altering the temperature and water vapor fraction states in the airway.

In this study, steady-state simulation was performed at a constant breathing rate. Constant flow rates of 5, 10, and 20 L/min were set to match the scenarios in Rouadi et al.[3] for verifying the subwall model. We chose not to compare against the dataset of[1] as the measurements were taken at the end of inspiration and the flow conditions are incompatible with a steady state simulation. For example, the end of inspiration temperature is influenced by hysteresis effects from a higher temperature source during exhalation. At peak exhalation the free stream temperature inside the nasal cavity is close to alveoli conditions until inhalation begins. Heat transfer only takes place when inhalation starts. Furthermore, the flow rate is oscillatory during breathing with a very low flow rate at the end of inhalation.

Nevertheless, the three additional inhalation cases were simulated with a constant flow rate of 15 L/min which can serve as a representative flow field for the inherent cyclic nature of breathing. This assumption is based on the Womersley number approximately equal to 1.7 suggesting the quasi-steady flow modeling approach is valid for describing the averaged flow field.[35,36] Nevertheless, real breathing flow is not steady. Doorly et al.[35] state where hysteresis is manifested over the inspiratory (and expiratory) period, a steady state model is inappropriate, and reproduction of transient effects are necessary for accumulative processes (deposition, heat transfer).

Further limitations of this study include: individual anatomical (e.g., geometry) differences among patient can produce different flow fields; and heterogeneity of core temperature and humidity in the submucosal regions of the nasal cavity.

5 | CONCLUSION

The air conditioning capacity of the nasal cavity is governed by heat and mass transfer. The heat transfer occurs from the temperature difference between the inhaled air temperature and the internal mucosal wall temperature, while the mass transfer occurs from the difference between the water vapor fraction of the inhaled air, and the continuously wet mucosal surface. In the latter process the energy required for evaporation is in the form of the latent heat of vaporization of water. This work expands on existing modeling efforts in accounting for the dual heat and mass transfer process in the nasal cavity by introducing a new subwall model that accounts for the evaporative cooling effect. A pipe geometry was firstly used to demonstrate the evaporative cooling principle. A human nasal cavity model was recreated from CT-scans and six inhalation conditions were evaluated. This included three steady state inhalation conditions obtained from the experimental data of Rouadi et al.,[3] and cold dry air, normal air, and hot humid air. The results demonstrated a cooler mucosal surface temperature when latent heat exchange was included. Among the six cases, the amount of energy from sensible heat ranged from 0.1 to 10.5 W, and from latent heat ranged from 3.6 to 20.0 W. The current work applied a steady solution on a single patient specific nasal cavity. However, the subwall model can be applied to other engineering applications that involve evaporation, such as a swimming pool, human thermal conditions from perspiration, and evaporative coolers.

CONFLICT OF INTEREST
The authors declare no conflicts of interest.

DATA AVAILABILITY STATEMENT
The data that supports the findings of this study are available in the supplementary material of this article.

ORCID
Kiao Inthavong https://orcid.org/0000-0003-0476-0237
David F. Fletcher https://orcid.org/0000-0003-2221-4192
Mehrdad Khamooshi https://orcid.org/0000-0002-1600-7085
Sara Vahaji https://orcid.org/0000-0001-6047-2163
Hana Salati https://orcid.org/0000-0002-9404-2417

REFERENCES
1. Keck T, Leiacker R, Riechelmann H, Rettinger G. Temperature profile in the nasal cavity. *Laryngoscope*. 2000;110(4):651-654.
2. Keck T, Leiacker R, Heinrich A, Kühnemann S, Rettinger G. Humidity and temperature profile in the nasal cavity. *Rhinology*. 2000; 38(4):167-171.
3. Rouadi P, Baroody FM, Abbott D, Naureckas E, Solway J, Naclerio RM. A technique to measure the ability of the human nose to warm and humidify air. *J Appl Physiol*. 1999;87(1):400-406.
4. Lindemann J, Leiacker R, Rettinger G, Keck T. Nasal mucosal temperature during respiration. *Clin Otolaryngol Allied Sci*. 2002;27(3):135-139.
5. Bailey RS, Casey KP, Pawar SS, Garcia GJ. Correlation of nasal mucosal temperature with subjective nasal patency in healthy individuals. *JAMA Facial Plastic Surg*. 2017;19(1):46-52.
6. Tsakiropoulou E, Vital V, Constantinidis J, Kekes G. Nasal air-conditioning after partial turbinectomy: myths versus facts. *Am J Rhinol Allergy*. 2015;29(2):59-62.
7. Lindemann J, Leiacker R, Sikora T, Rettinger G, Keck T. Impact of unilateral sinus surgery with resection of the turbinates by means of midfacial degloving on nasal air conditioning. *Laryngoscope*. 2002;112(11):2062-2066.
8. Wiesmiller K, Keck T, Rettinger G, Leiacker R, Dzida R, Lindemann J. Nasal air conditioning in patients before and after septoplasty with bilateral turbinoplasty. *Laryngoscope*. 2006;116(6):890-894.
9. Lindemann J, Leiacker R, Stehmer V, Rettinger G, Keck T. Intranasal temperature and humidity profile in patients with nasal septal perforation before and after surgical closure. *Clin Otolaryngol Allied Sci*. 2001;26(5):433-437.
10. Keck T, Leiacker R, Kühnemann S, Rettinger G. Heating of air in the nasal airways in patients with chronic sinus disease before and after sinus surgery. *Clin Otolaryngol Allied Sci*. 2001;26(1):53-58.

11. Lindemann J, Keck T, Wiesmiller K, et al. A numerical simulation of intranasal air temperature during inspiration. *Laryngoscope*. 2004; 114(6):1037-1041.

12. Lindemann J, Keck T, Wiesmiller K, et al. Nasal air temperature and airflow during respiration in numerical simulation based on multislice computed tomography scan. *Am J Rhinol*. 2006;20(2):219-223.

13. Inthavong K, Wen J, Tu J, Tian Z. From CT scans to CFD modelling–fluid and heat transfer in a realistic human nasal cavity. *Eng Appl Comput Fluid Mechan*. 2009;3(3):321-335.

14. Naftali S, Rosenfeld M, Wolf M, Elad D. The air-conditioning capacity of the human nose. *Ann Biomed Eng*. 2005;33(4):545-553.

15. Burgos M, Sanmiguel-Rojas E, Del Pino C, Sevilla-García M, Esteban-Ortega F. New CFD tools to evaluate nasal airflow. *Eur Arch Otorhinolaryngol*. 2017;274(8):3121-3128.

16. Inthavong K, Ma J, Shang Y, et al. Geometry and airflow dynamics analysis in the nasal cavity during inhalation. *Clin Biomechan*. 2019; 66:97-106.

17. Ma J, Dong J, Shang Y, Inthavong K, Tu J, Frank-Ito DO. Air conditioning analysis among human nasal passages with anterior anatomical variations. *Med Eng Phys*. 2018;57:19-28.

18. Ito K, Mitsumune K, Kuga K, Phuong NL, Tani K, Inthavong K. Prediction of convective heat transfer coefficients for the upper respiratory tracts of rat, dog, monkey, and humans. *Indoor Built Environ*. 2017;26(6):828-840.

19. Salati H, Khamooshi M, Vahaji S, Christo FC, Fletcher DF, Inthavong K. N95 respirator mask breathing leads to excessive carbon dioxide inhalation and reduced heat transfer in a human nasal cavity. *Phys Fluids*. 2021;33(8):081913.

20. Chen XB, Lee HP, Hin Chong VF, Wang DY. Assessment of septal deviation effects on nasal air flow: a computational fluid dynamics model. *Laryngoscope*. 2009;119(9):1730-1736.

21. Sullivan CD, Garcia GJ, Frank-Ito DO, Kimbell JS, Rhee JS. Perception of better nasal patency correlates with increased mucosal cooling after surgery for nasal obstruction. *Otolaryngol Head Neck Surg*. 2014;150(1):139-147.

22. Dayal A, Rhee JS, Garcia GJ. Impact of middle versus inferior total turbinectomy on nasal aerodynamics. *Otolaryngol Head Neck Surg*. 2016;155(3):518-525.

23. Garcia GJ, Bailie N, Martins DA, Kimbell JS. Atrophic rhinitis: a CFD study of air conditioning in the nasal cavity. *J Appl Physiol*. 2007; 103(3):1082-1092.

24. Kumahata K, Mori F, Ishikawa S, Matsuzawa T. Nasal flow simulation using heat and humidity models. *J Biomechan Sci Eng*. 2010;5(5): 565-577.

25. Kim DW, Chung SK, Na Y. Numerical study on the air conditioning characteristics of the human nasal cavity. *Comput Biol Med*. 2017;86:18-30.

26. Chung SK, Na Y. Dynamic characteristics of heat capacity of the human nasal cavity during a respiratory cycle. *Respir Physiol Neurobiol*. 2021;290:103674.

27. Hanida S, Mori F, Kumahata K, Watanabe M, Ishikawa S, Matsuzawa T. Influence of latent heat in the nasal cavity. *J Biomechan Sci Eng*. 2013;8(3):209-224.

28. Shrestha K, Salati H, Fletcher D, Singh N, Inthavong K. Effects of head tilt on squeeze-bottle nasal irrigation–a computational fluid dynamics study. *J Biomech*. 2021;123:110490.

29. Zhang Y, Shang Y, Inthavong K, et al. Computational investigation of dust mite allergens in a realistic human nasal cavity. *Inhal Toxicol*. 2019;31(6):224-235.

30. Na Y, Chung SK, Byun S. Numerical study on the heat-recovery capacity of the human nasal cavity during expiration. *Comput Biol Med*. 2020;126:103992.

31. Beule AG. Physiology and pathophysiology of respiratory mucosa of the nose and the paranasal sinuses. *GMS Curr Top Otorhinolaryngol Head Neck Surg*. 2010;9:Doc07.

32. Senanayake P, Salati H, Wong E, et al. The impact of nasal adhesions on airflow and mucosal cooling-a computational fluid dynamics analysis. *Respir Physiol Neurobiol*. 2021;293:103719.

33. Calmet H, Inthavong K, Owen H, et al. Computational modelling of nasal respiratory flow. *Comput Meth Biomech Biomed Eng*. 2020; 24(4):1-19.

34. Keck T, Lindemann J. Numerical simulation and nasal air-conditioning. *GMS Current Topics in Otorhinolaryngol Head Neck Surg*. 2010; 9:Doc08.

35. Doorly D, Taylor D, Schroter R. Mechanics of airflow in the human nasal airways. *Respir Physiol Neurobiol*. 2008;163(1–3):100-110.

36. Inthavong K, Das P, Singh N, Sznitman J. In silico approaches to respiratory nasal flows: a review. *J Biomech*. 2019;97:109434.

SUPPORTING INFORMATION

Additional supporting information may be found in the online version of the article at the publisher's website.